

Phonon thermal Hall as a lattice Aharonov-Bohm effect

Kamran Behnia^{1*}

1 Laboratoire de Physique et d'Étude des Matériaux
(ESPCI - CNRS - Sorbonne Université)
Université Paris Sciences et Lettres, 75005 Paris, France

* kamran.behnia@espci.fr

Abstract

In a growing list of insulators, experiments find that magnetic field induces a misalignment between the heat flux and the thermal gradient vectors. This phenomenon, known as the phonon thermal Hall effect, implies energy flow without entropy production along the orientation perpendicular to the temperature gradient. The experimentally-measured thermal Hall angle in various insulators does not exceed a bound and becomes maximal at the temperature of peak longitudinal thermal conductivity. The present paper aims to propose a scenario providing and explanation for these two experimental facts. It begins by noticing that at this temperature, T_{max} , Normal phonon-phonon collisions become most frequent in comparison with Umklapp and boundary scattering events. Furthermore, the Born-Oppenheimer approximated molecular wave functions are known to acquire a phase in the presence of a magnetic field. In an anharmonic crystal, in which tensile and compressive strain do not cancel out, this field-induced atomic phase gives rise to a phonon Berry phase and generates phonon-phonon interference. The rough amplitude of the thermal Hall angle expected in this picture is set by the phonon wavelength, λ_{ph} , and the crest atomic displacement, δu_m at T_{max} . The derived expression is surprisingly close to what has been experimentally found in black phosphorus, germanium and silicon.

Contents

1	Introduction	2
2	On the significance of a thermal Hall angle	4
3	Anharmonicity and phonon-phonon collisions	5
4	Molecular Aharonov- Bohm effect and the Born-Oppenheimer approximation in a magnetic field	9
5	Field-induced geometric phase of phonons	11
6	Normal collisions between complex phonons	13
7	Comparison between the expected and the observed amplitudes of the thermal Hall angle	15
8	Concluding remarks	16

9 Acknowledgments	17
References	17

1 Introduction

Discovered almost two decades ago [1], the phonon Hall effect has attracted an intense attention in recent years. Nowadays, there is a long list of insulators in which the effect has been experimentally observed [2–17]. There is also an ample literature of theoretical proposals [18–26]. This field of investigation overlaps with others exploring the chirality and the angular momentum of phonons as well as their coupling with magnetism [27, 28].

The recent observation of phonon thermal Hall effect in elemental and non-magnetic insulators (phosphorus [12], silicon [15] and germanium [15]), however, indicates that this is a fairly common phenomenon [29]. There appears to be a fundamental flaw in our understanding of heat propagation in insulators. This is surprising, because *ab initio* calculations have achieved an account of the experimentally measured thermal conductivity in silicon and other insulators within percent accuracy [30]. This remarkable accomplishment of computational solid-state physics implies that the phonon spectrum and phonon-phonon interactions are well understood. The unexpected phonon Hall response indicates that a crucial detail is overlooked in our fundamental picture of heat conduction in insulators [31, 32].

This paper proposes to find this missing element by looking at the consequences of an alliance between anharmonicity and non-adiabaticity. The idea is that an account of the phonon thermal Hall effect can be found by going beyond the harmonic and the adiabatic approximations [intriguingly treated next to each other in the textbook by Aschcroft and Mermin] [33].

Anharmonicity refers to the fact that the interatomic restoring force is not simply proportional to the atomic displacement. This is not exotic. All known solids are anharmonic with third-order elastic constants. Adiabaticity refers to the separation of the electronic and the nuclear motions driven by a large mass discrepancy, and warranted by the Born-Oppenheimer approximation [34]. It is known to break down in the presence of a magnetic field [35, 36]. The molecular Aharonov Bohm-effect [37, 38] is a demonstration that the nuclear and the electronic wavefunctions can become complex functions of space and time. I will argue that, in any anharmonic crystal, the field-induced phase of atoms and molecules [35, 36], will give rise to a geometric [Berry] phase [39–42] to ordinary acoustic phonons. By altering Normal collisions between phonons, this can generate a thermal Hall signal of an amplitude much larger than what was proposed before [43].

Figure 1 shows two experimental features, reported in previous studies and motivating the present paper. Panel a displays the reported data [12, 15] for three elemental insulators. Panel b is reproduced from ref. [44].

Fig. 1a shows the temperature dependence of the longitudinal, κ_{ii} , and the transverse (i.e. Hall), κ_{ij} , thermal conductivities of silicon, germanium and black phosphorus. κ_{ii} and κ_{ij} are both normalized to their peak value in order to make an observation: *The thermal Hall signal peaks where the longitudinal thermal conductivity peaks and it decreases faster on both sides of the peak.* This is broadly true of all other cases (See Figure 3 in ref. [12]). We will call this material-dependent temperature T_{max} and focus on the three elemental solids, because their longitudinal thermal conductivity is understood in great detail [30].

Fig. 1b shows the amplitude of the maximum κ_{ij} in several insulators divided by the magnetic field at which it was measured as a function of their maximum κ_{ii} . The sign of κ_{ij}

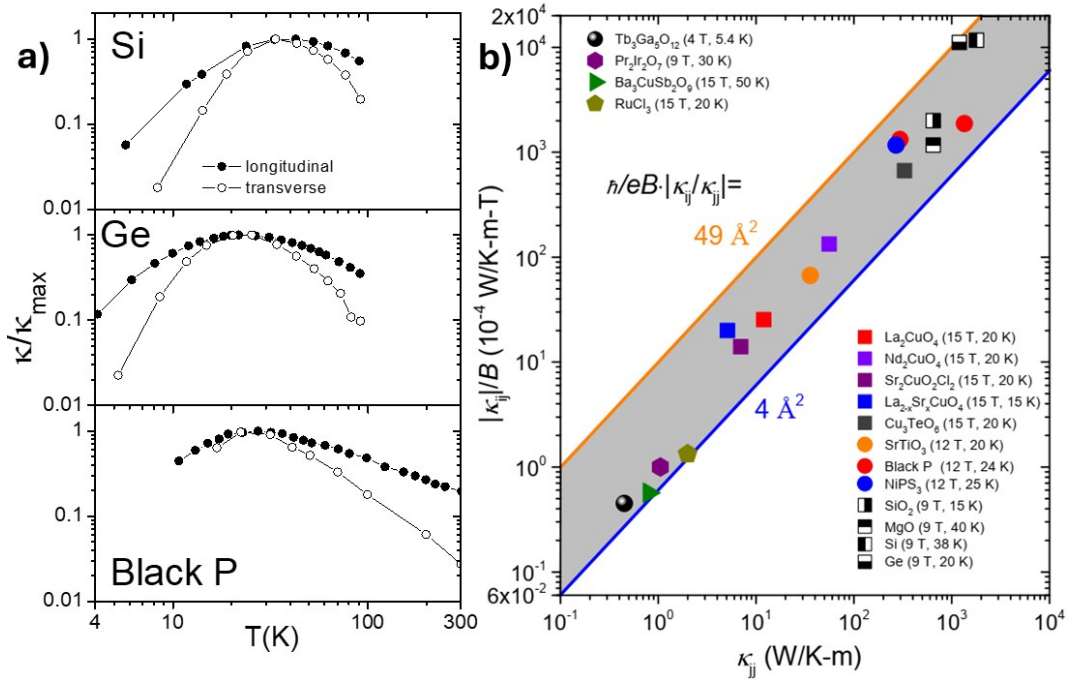


Figure 1: a) Transverse and longitudinal thermal conductivities in three elemental insulators normalized by their peak amplitude. The two conductivities peak at the same temperature and the transverse response decreases faster at both the warmer and the colder sides of the peak. b) The peak thermal Hall conductivity divided by magnetic field in a variety of insulators as a function of their maximum longitudinal thermal conductivity. While the latter varies by four orders of magnitude, the former remains proportional to it and their ratio displays little change.

is neglected in this plot. One can see that κ_{ii} changes by more than four orders of magnitude, which indicates that the phonon mean free path is very different in these insulators. The cleanest, as well as the simplest, are elemental (Si Ge and P). Their data symbols are located on the right side of the figure. The dirtiest and the most complex are on the left. Remarkably, the peak amplitudes of κ_{ij} and κ_{ii} correlate with each other. In order words, *their ratio, the tangent of the Hall angle, does not exceed an upper bound*. Since the ratio remains small in laboratory magnetic fields (≤ 0.01 in a magnetic field of ~ 10 T), we will simply call the ratio the thermal Hall angle. Using fundamental constants, this ratio can be translated to a length scale. As seen in the figure, this length scale does not correlate with the phonon mean free path, which sets the maximum κ_{ii} .

The focus of the present are insulators in which any spin-phonon coupling is absent and there is no magnetic contribution to the thermal Hall effect. This does not mean that such effects are absent in some of the materials included in Fig. 1b. Most probably, in presence of magnetism, other contributions to the thermal Hall conductivity may arise. Restricting ourselves to non-magnetic insulators, in which phonons are alone (both as carriers and as intrinsic scattering centers) let us try to address two questions : Why does the thermal Hall angle peak at T_{\max} , (Fig. 1.a)? Why its amplitude appear to be bounded by length scales other than phonon mean free path and common to numerous solids (Fig. 1.b) ?

The paper is organized as follows. Section 2 puts the notion of thermal Hall angle under scrutiny. A misalignment between the thermal gradient and the heat current density vectors implies a flow of heat without entropy production. As a consequence, the thermal Hall angle

acts like the efficiency of a thermal machine, reminiscent of the Brownian ratchet introduced by Smoluchowski and popularized by Feynman [45]. Section 3 is devoted to anharmonicity. It argues that Normal phonon-phonon collisions become most prominent when $T \approx T_{max}$. Section 4 is devoted to the fate of the Born-Oppenheimer approximation in the presence of magnetic field. It recalls that the molecular Aharonov-Bohm effect was the first case of geometric (Berry) phase [39, 40, 42]. In a magnetic field, atoms, molecules are expected to have a geometric phase. In section 5, we will see that in an anharmonic crystal, this will generate a phase for phonons. Section 6 considers how this latter phase can weigh on collisions between phonons and lead to a Hall signal. Finally, section 7 gives a rough estimation of the expected signal, which happens to be in good agreement with the experimental observation.

2 On the significance of a thermal Hall angle

Figure 2a is a sketch of a standard set-up for measuring the thermal Hall effect. The sample is sandwiched between a heater and a cold finger. This fixes the orientation of the heat density current, \vec{J}_q . Three thermometers (resistive chips or thermocouples) measure the local temperature at three different points of the sample. The difference between them leads to the quantification of the temperature gradient along \vec{J}_q and perpendicular to it. The ratio of these two thermal gradients is no other than the tangent of the thermal Hall angle and identical to the ratio of off-diagonal to diagonal conductivity [or resistivity].

When the experiment finds a genuine difference between the local temperatures recorded by the two thermometers T_1 and T_2 of Figure 2a, there is a finite thermal Hall signal. It implies an angle between the two vectors \vec{J}_q and $\vec{\nabla}T$ (Figure 2b) and therefore a process in which

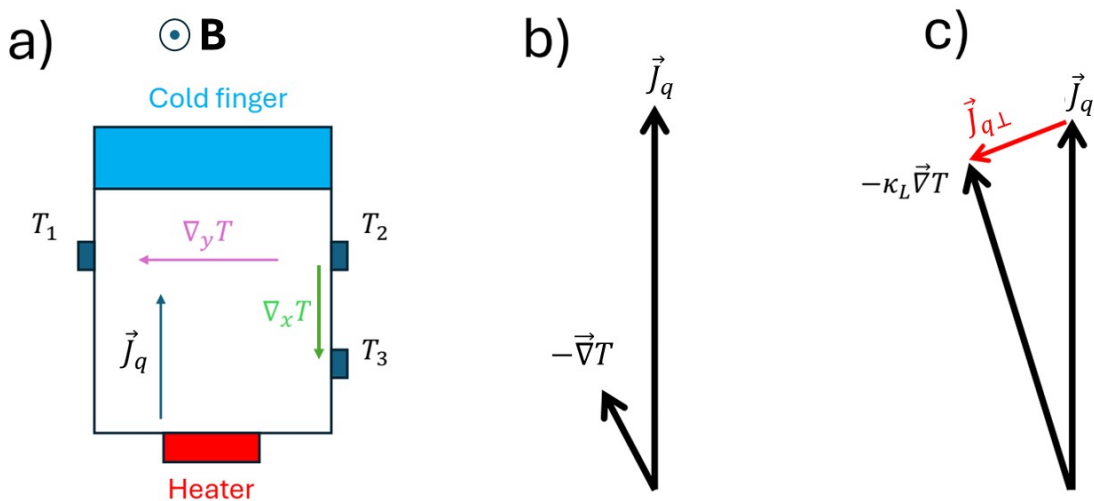


Figure 2: a) In a thermal Hall experiment, the sample is held between a heater and a cold finger. This allows to establish a finite heat current density vector, \vec{J}_q , along an orientation, which is often a crystallographic axis. Three temperature sensors allow measuring the temperature gradient along two orientations, which are parallel ($\nabla_x T$) and perpendicular ($\nabla_y T$) to \vec{J}_q . b) A finite $\nabla_y T$ means that there is a misalignment between the thermal gradient vector, $\vec{\nabla}T$ and \vec{J}_q . c) Such a misalignment implies a heat flow without entropy production in the direction perpendicular to $\vec{\nabla}T$.

thermal energy flows without producing any entropy.

A temperature gradient implies entropy production. Textbooks devoted to non-equilibrium thermodynamics [46, 47] assume an ‘entropy source’, σ^s , which quantifies the rate of entropy production per unit volume (units : W.K⁻¹m⁻³). σ^s is related to the entropy current density, $\vec{J}_s = \frac{\vec{J}_q}{T}$ by :

$$\sigma^s = \vec{\nabla} \cdot \vec{J}_s \quad (1)$$

The experimentally accessible quantity \vec{J}_q is also linked to σ^s [46, 47]:

$$\sigma^s = \vec{J}_q \cdot \vec{\nabla} \frac{1}{T} + \sum_{\alpha} J_{\alpha} X_{\alpha} \cdot s \quad (2)$$

Here, J_{α} (X_{α}) is an Onsager force (flux). The right hand side of this equation singles out a unique force-flux pair, namely $\vec{\nabla} \frac{1}{T}$ (the thermal force) and \vec{J}_q (the thermal flux). Neglecting thermodynamic forces and fluxes associated with flow of matter and charge:

$$\sigma^s = \frac{1}{T^2} \vec{J}_q \cdot \vec{\nabla} T. \quad (3)$$

Equation 3 states that entropy production is the scalar product of the two vectors. When these two (\vec{J}_q and $\vec{\nabla} T$) are not parallel to each other, a component of \vec{J}_q , which is perpendicular to $\vec{\nabla} T$, does not produce entropy (Figure 2c).

The efficiency of this engine can be defined as $\eta = J_{q\perp}/J_q$. It is easy to see that the tangent of the Hall angle, $\tan \Theta_H = \frac{\nabla_y T}{\nabla_x T}$, is linked to η , the sinus of the same angle, and therefore:

$$\tan \Theta_H = \frac{\eta}{\sqrt{1 - \eta^2}} \quad (4)$$

Experimentally, $\tan \Theta_H \ll 1$ and $\Theta_H \approx \eta$ is a good approximation, making the experimentally observed thermal Hall angle akin to an efficiency.

This situation is reminiscent of a Brownian ratchet [48, 49], introduced by Smoluchowski and popularized by Feynman in his famous lectures [45]. The original design consisted of a ratchet with a pawl and a spring (capable of rectification) coupled to a wheel which can rotate either clock-wise or anti-clockwise. However, the design can be simplified to any pairs of rectifier and non-rectifier Brownian ‘particles’ coupled to each other and kept at different temperatures [50]. Such an engine generates work with an efficiency below the Carnot efficiency [51].

There is a finite thermal Hall angle in an insulator when magnetic field becomes a rectifier inside a phonon gas subject to a temperature gradient. There is an obvious parenthood with the variety of stochastic ratchets combining thermal Noise and asymmetric potential [49]. Because of the fundamental differences between the phonon gas and a real gas, such an analogy has limits. The phonon number is not preserved and the group velocity of acoustic phonons does not depend on temperature. In contrast to a real gas, the flow of heat in a phonon gas is accompanied by a net flow of phonons. As we will see below, the magnetic field can become a ‘ratchet’ in this context.

3 Anharmonicity and phonon-phonon collisions

The harmonic approximation cannot explain the finite thermal expansion and the finite thermal resistivity of solids [33]. These are common features of real solids. Therefore, anharmonicity is widespread. Second-order elastic constants, defined by the linear relationships

between strains and stresses, suffice for description of harmonic properties. On the other hand, higher-order elastic constants [52] are required to describe anharmonicity.

Discussing the origin of the negative thermal expansion of silicon between $\simeq 10$ K and $\simeq 120$ K [53], Kim and co-workers [54] distinguish between ‘pure anharmonicity’, associated with finite cubic and quartic elastic constants, and ‘quasi-harmonicity’, which assumes harmonic oscillators with volume-dependent frequencies. The latter can be captured by a finite Grüneisen parameter ($\gamma_i = \frac{V\partial\omega_i}{\omega_i\partial V}$) [33] and can be used to account for a thermal expansion of both signs. In contrast, an account of thermal resistivity requires invoking ‘pure anharmonicity’ and higher order terms in the interatomic potential. In this way, the energy of a phonon is altered by the presence of other phonons, irrespective of any change in the volume [54].

In their textbook [55], Hook and Hall give the following account of how phonons couple to each other. If strain modifies sound velocity, a traveling sound wave cannot remain indifferent to the presence of another sound wave. The coupling will show up in the phase modulation of the wavefront. Imagine a traveling phonon with a frequency of ω_1 and a wave-vector of \vec{q}_1 :

$$A = \text{Re}[e^{i(\vec{q}_1 \cdot \vec{r} - \omega_1 t)}] \quad (5)$$

Now, the presence of a phonon with a frequency of ω_2 and wave-vector of \vec{q}_2 will modulate the phase of the first phonon [55]:

$$A = \text{Re}[e^{i(\vec{q}_1 \cdot \vec{r} - \omega_1 t + C \cos(\vec{q}_2 \cdot \vec{r} - \omega_2 t))}] \quad (6)$$

Hook and Hall introduced the dimensionless parameter C , which represents the strength of anharmonicity. Since $C \ll 1$, one can replace the exponential in equation 6 with its expansion :

$$A = \text{Re}[e^{i(\vec{q}_1 \cdot \vec{r} - \omega_1 t)}[1 + iC \cos(\vec{q}_2 \cdot \vec{r} - \omega_2 t) + \dots]] \quad (7)$$

Neglecting the higher terms, the expansion becomes:

$$\begin{aligned} A \simeq \text{Re}[e^{i(\vec{q}_1 \cdot \vec{r} - \omega_1 t)} &+ \frac{1}{2} C i e^{i[(\vec{q}_1 + \vec{q}_2) \cdot \vec{r} - (\omega_1 + \omega_2)t]} \\ &+ \frac{1}{2} C i e^{i[(\vec{q}_1 - \vec{q}_2) \cdot \vec{r} - (\omega_1 - \omega_2)t]}] \end{aligned} \quad (8)$$

The amplitude of this wave is real and can be expressed as:

$$\begin{aligned} A \simeq \cos(\vec{q}_1 \cdot \vec{r} - \omega_1 t) - & \\ \frac{1}{2} C [\sin[(\vec{q}_1 + \vec{q}_2) \cdot \vec{r} - (\omega_1 + \omega_2)t] - & \\ \sin[(\vec{q}_1 - \vec{q}_2) \cdot \vec{r} - (\omega_1 - \omega_2)t]] \end{aligned} \quad (9)$$

The first term of this equation represents the original wave with ω_1 and \vec{q}_1 as frequency and wave-vector. The two other terms represent two new waves with identical amplitudes and phase shifts ($\pi/2$). The first has a frequency and a wave-vector of:

$$\vec{q}_3 = \vec{q}_1 + \vec{q}_2; \omega_3 = \omega_1 + \omega_2 \quad (10)$$

The frequency and the wave-vector of the other one are:

$$\vec{q}_3 = \vec{q}_1 - \vec{q}_2; \omega_3 = \omega_1 - \omega_2 \quad (11)$$

These equations represent three-phonon processes, in which a third phonon is created either by absorption or by emission. The four-phonon terms ($\mathcal{O}(C^2)$), known to matter in many crystals [56], will be neglected, for the sake of simplicity.

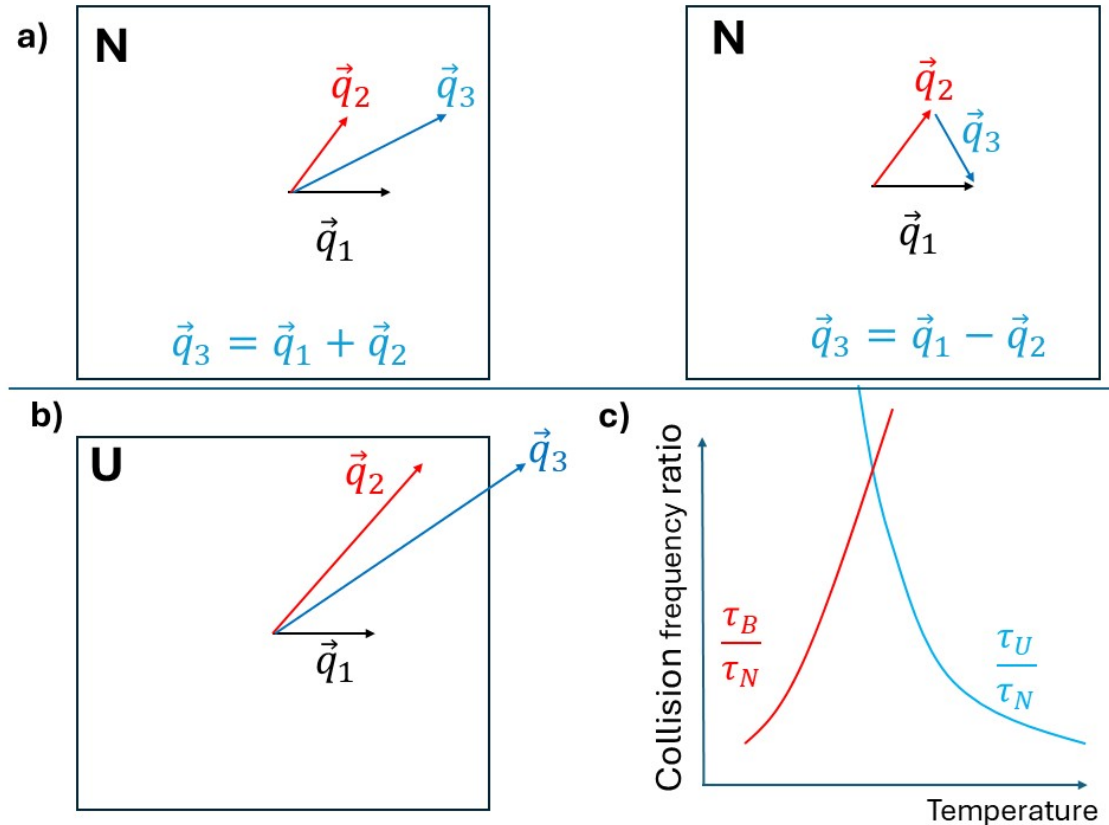


Figure 3: a) Two kinds of three-phonon Normal collisions. A phonon with a \mathbf{q}_1 wave-vector can absorb another phonon with a wave-vector \mathbf{q}_2 (left) or emit a phonon with a wave-vector \mathbf{q}_2 (right). These two Normal events can be transformed one to another by permuting the initial (\mathbf{q}_1) and the final (\mathbf{q}_3) phonons. They do not produce entropy. (b) When the sum of the wave-vector of the colliding phonons is sufficiently large, their collision is an Umklapp event, which generates entropy. Here the \mathbf{q}_3 phonon is forbidden by the discrete symmetry of the crystal. (c) The relative frequency of Normal collisions respective to Umklapp and boundary scattering. At the peak temperature, the chance of a thermally excited phonon to suffer a Normal scattering event is the largest.

Hooke and Hall end their derivations of equations 10 and 11 by commenting that they are “more correctly regarded as a geometrical interference condition... than as a conservation law for momentum.”

Absorption and emission events are distinct only in the presence of an arrow of time. If instead of beginning with \mathbf{q}_1 and ending with \mathbf{q}_3 one begins with the latter and ends with the former, an emission event becomes an absorption event and vice versa. Such events do not produce entropy. However, there are ph-ph scattering events, which do produce entropy (See Fig. 3b). If \vec{q}_3 gets out of the Brillouin zone, the scattering event is known as Umklapp. Since a lattice cannot host a sound wave with a wavelength shorter than twice the interatomic distance, a , it is impossible to have $|\vec{q}_3| > \frac{\pi}{a}$. When this is the case, a fraction of the quasi-momentum is absorbed by the crystal. Note that in this case, there is no way to start with the

forbidden final wave-vector.

The distinction between Normal and Umklapp events is not clearcut when $|\vec{q}_3| \approx \frac{\pi}{a}$ [55, 57]. However, despite this fuzziness, the statistical distinction keeps its conceptual utility for distinguishing between different heat transport regimes.

Phonon-phonon scattering is the main source of thermal resistivity at high temperature. At low temperatures, the wave-vector of thermally excited phonons is too short for Umklapp events. The major source of entropy production, absent large-scale disorder, is boundary scattering [31–33, 55]. Experiments find that at low temperature (that is $T \ll T_{max}$), the thermal conductivity in clean crystals is set by sample size irrespective of the presence of point-like defects (chemical and isotopic impurities) [32]. The extracted phonon mean free path is of the order of the sample thickness, therefore phonons travel ballistically.

Thus, in a perfect but finite crystal, there are two ways to produce entropy despite wave-like propagation. Either through boundary scattering or by generating a wavelength disallowed by the lattice discrete symmetry. These two routes for dissipation set the temperature dependence of the longitudinal thermal conductivity. It increases with cooling when the main driver of resistivity is Umklapp phonon-phonon scattering (which rarefies as the wave-vectors of colliding phonons shrink). It decreases with cooling when it is dominated by boundary scattering rate (due to the change in phonon population). The peak of thermal conductivity occurs when the two regimes, ballistic-extrinsic (low temperature and dominated by sample size) and the diffusive-intrinsic (high temperature and dominated by ph-ph collisions) meet.

This picture is to be complemented by considering the occurrence of Normal scattering events. As early as 1966, Guyer and Krumhansl [58] identified four distinct regimes of thermal transport regimes as a function of the hierarchy between different scattering times, including the one associated with Normal events. In addition to the ballistic and diffusive regimes discussed above, in the vicinity of the peak thermal conductivity, hydrodynamic regimes driven by Normal collisions between phonons have been postulated [58–60] and experimentally detected in a variety of insulators [61–67].

The time between two Normal events, τ_N , and the time between two Umklapp events, τ_U , decrease with warming. In both cases, there are simply more phonons and more collisions at high temperature. However, τ_U decreases faster because it includes an additional factor due to the change in the typical phonon wave-vector. Therefore τ_U/τ_N decreases with warming. The time scale for boundary scattering is the ratio of sample size to sound velocity ($\tau_B \simeq d/v_s$) and is roughly temperature-independent. Therefore, τ_B/τ_N increases with warming (Fig.3c). Now, thermal conductivity peaks at the cross-over between the intrinsic and scattering regimes of scattering, where Normal scattering events, which do not produce entropy can weigh most (Fig.3b). Warming above temperature would reduce their frequency compared to Umklapp events. Cooling below this temperature would disfavor them in the face of competition by boundary scattering.

This simplified picture ignores the multiplicity of phonon modes with distinct velocities and the frequency dependence of τ_U and τ_N . These subtleties notwithstanding, it is safe to assume the prominence of Normal phonon-phonon collisions near the peak. Indeed, hydrodynamic features have been observed near this peak by steady-state thermal transport experiments in many clean insulators [59, 61–65]. The detection of these features require a specific hierarchy ($\tau_U > \tau_B > \tau_N$) of time scales.

The thermal Hall angle (which requires a flow of phonons without entropy production) peaks at the temperature at which Normal phonon-phonon scattering (which does not produce entropy) are most prominent. It is tempting to make a connection between the two. But how can the magnetic field influence collisions between phonons?

4 Molecular Aharonov- Bohm effect and the Born-Oppenheimer approximation in a magnetic field

For almost a century, the Born-Oppenheimer (BO) approximation [34] has been a cornerstone of molecular physics and chemistry. Since the atomic mass, M exceeds by far the electron mass μ , the solution to the time-independent Schrödinger equation is expanded in orders of μ/M ratio. This allows disentangling the electronic and the nuclear motions. First, the electronic problem for fixed nuclei is solved. The higher orders of the expansion can then be used to quantify nuclear vibrations (phonons in a crystal) as well as their coupling to the electronic degrees of freedom [68–71]. In this approach, there is an Adiabatic Potential Energy Surface (APES) of electrons setting the nuclear trajectory.

The BO approximation is known to break down when the mixing of different electronic states cannot be ignored, as in the case of Jahn-Teller effect [72].

Interestingly, one of the first identified manifestations of the Berry's phase [40] was the so-called “molecular Aharonov-Bohm effect” [38, 73], which occurs in the presence of a conical intersection between potential energy surfaces [74]. By making the electronic energy levels doubly degenerate, this can be pictured as a fictitious magnetic field. Let us represent the nuclear coordinates by \mathbf{R} . In the BO approximation, an energy eigen-state, $|\Psi(\mathbf{R})\rangle$ is assumed to be the product of a nuclear wavefunction $\psi(\mathbf{R})$ and an electronic ket depending on \mathbf{R} , $|\chi(\mathbf{R})\rangle$:

$$|\Psi(\mathbf{R})\rangle \approx |\chi(\mathbf{R})\rangle\psi(\mathbf{R}) \quad (12)$$

Mead proposed distinguishing between a nuclear momentum operator, $\hat{P} = -i\hbar\nabla_{\mathbf{R}}$, the conjugate of the position operator for the total wavefunction, $|\Psi(\mathbf{R})\rangle$, and an effective momentum operator, $\hat{\Pi}$, operating on $\psi(\mathbf{R})$. Their relationship can be written as [38]:

$$\hat{\Pi}\psi(\mathbf{R}) = \langle\chi(\mathbf{R})|\hat{P}|\Psi(\mathbf{R})\rangle \quad (13)$$

Making the right hand side of the equation explicit leads to the following expression for nuclear momentum [38]:

$$\langle\chi(\mathbf{R})|(-i\hbar\nabla_{\mathbf{R}})|\Psi(\mathbf{R})\rangle = -i\hbar[\nabla_{\mathbf{R}}\Psi(\mathbf{R}) + \langle\chi(\mathbf{R})|\nabla_{\mathbf{R}}\chi(\mathbf{R})\rangle] \quad (14)$$

The second term in the right hand side of this equation is recognizable as a Berry connection. If $\langle\chi(\mathbf{R})|\nabla_{\mathbf{R}}\chi(\mathbf{R})\rangle$ is zero, there is no need to worry about the phase. However, when it becomes finite, the nuclei trajectory has a ‘geometric vector potential’. In this case, the wavefunction cannot be treated as a real number [38]. Mead dubbed this effect ‘the molecular Aharonov-Bohm effect’ [37], referring to the celebrated proposal by Aharonov and Bohm in 1959 [75], in which the magnetic vector potential and the phase of the wavefunction play prominent roles.

The presence of a genuine magnetic field makes a qualitative difference. As Resta pointed out [40], in addition to a *possible* geometric phase, there is an *unavoidable* one, induced by magnetic field. In 1988, Schmelcher, Cederbaum and Meyer investigated BO approximation in the presence of the magnetic field. They found that the simple extension of zero-field Born-Oppenheimer adiabatic approximation with no modification would make nuclei appear as “naked” charges, i.e., with no screening of the magnetic field by the electrons. This led them to distinguish between the diagonal and off-diagonal terms of the non-adiabatic coupling and formulate what they called the ‘screened Born-Oppenheimer approximation’ [35]. In 1992, Mead [38] argued that this approach originally identified as introducing “diagonal non-adiabatic correction” [35], and motivated by keeping gauge consistency, is equivalent to the addition of a geometric vector potential due to the finite magnetic field.

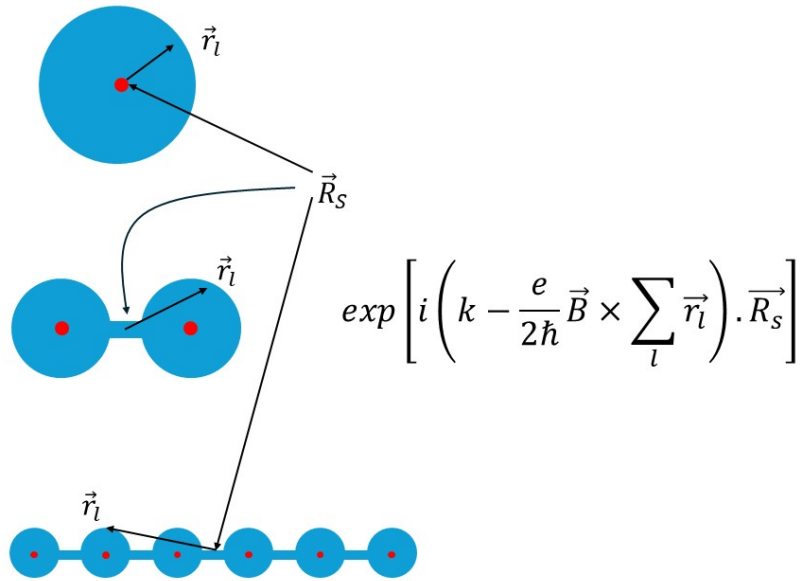


Figure 4: a) In the presence of magnetic field, an atom (top), a molecule (middle) and a chain of atoms (bottom) have a gauge-dependent phase. Expressed in the symmetric gauge, it is given by the vector product of the magnetic field and the coordinate of each electron with respect to the center of mass of the molecule. The position of the nuclei is absent in this expression, because they cancel out with respect to the center of mass.

Schmelcher *et al.* [35], using the symmetric gauge, $\mathbf{A}(\mathbf{r}) = \frac{1}{2}\mathbf{B} \times \mathbf{r}$, separate a phase factor of a homonuclear diatomic molecule correcting the pseudo-momentum, \vec{k} of the molecular wave-function:

$$\exp \left\{ [+i[\vec{k} - \frac{e}{2\hbar}(\vec{B} \times \sum_l \vec{r}_l)] \cdot \vec{R}_s] \right\} \quad (15)$$

Here \vec{r}_l represent the coordinates of the electron indexed l with respect to the center of mass of the molecule. The latter's coordinates are represented by \vec{R}_s .

This expression invites several comments. Its first remarkable feature is that it does not depend on the ratio of the electron-to-nucleus mass ratio. Note also that this expression is gauge-dependent and it remains to be seen that it has any observable consequences. Moreover, as illustrated in Fig. 4a, such a gauge-dependent phase factor is present in an atomic wave-function, or in the wave-function of a chain of atoms. In each case, one needs to shift the coordinate of the center-of-mass and set the amplitude of the pseudo-momentum as the sum of atomic pseudo-momenta [35]. Finally, let us note that this phase factor of Equation 15 is the ratio of two areas: ($\sum_l \mathbf{r}_l \cdot \mathbf{R}_s$ and ℓ_B^2 , with $\ell_B = \sqrt{\frac{\hbar}{eB}}$ being the magnetic length.)

The ultimate source of this phase factor is the difference in the distributions of the positive and negative charge. Heavier nuclei determine \vec{R}_s . On the other hand, the electronic cloud does not influence \vec{R}_s . Therefore, the sum of electronic positions with respect to the overall center of mass is not necessarily zero. The magnetic flux, which is gauge-invariant, do not affect the electron cloud and the point-like nuclei in the same way. The inherently complex

atomic wave-function in the presence of the magnetic field can yield a geometric phase to atomic vibrations.

5 Field-induced geometric phase of phonons

Recent *ab initio* molecular dynamic studies have uncovered consequences of the field-induced Berry phase in the presence of astrophysical magnetic fields [76–78]. The geometric vector potential was found to produce a significant screening force. In contrast, save for a noticeable exception [43], there is no record of such studies in crystals.

Combined with anharmonicity, this unavoidable field-induced phase will give rise to a phonon geometric phase, which is bounded by the following expression:

$$\delta\phi_B \approx q_e \frac{\lambda_{ph}\delta u_m}{\ell_B^2} \quad (16)$$

The two length scales in this expression, which is the main result of this paper, are the phonon wavelength, λ_{ph} , and the atomic displacement at the wave crest, δu_m . Their product defines an area quantifying atomic displacement off the equilibrium position. The ratio of this area to the square of the magnetic length, ℓ_B , quantifies the fraction of the quantum of the magnetic length contained in this area. These length scales are experimentally accessible. The dimensionless q_e is a real number, which depends on the anharmonicity of the crystal and is of the order of unity.

To see the origin of Equation 16, let us begin with a chain of centrosymmetric unit cells, each filled by a homogeneous electronic charge and a point-like nucleus at its center (See Figure 5 a). In equilibrium, the electronic and the nuclear center of mass superpose. Therefore, $\sum_l \vec{r}_l = 0$ and Equation 15 yields a zero phase everywhere. On the other hand, a collective vibration generates a mismatch between the nuclear and the electronic centers-of-mass giving rise to a finite local BO phase (Figure 5 a).

The subject matter of the first chapter of Ziman's textbook [80] is a similar atomic chain. The starting Hamiltonian is the following:

$$H = \frac{1}{2M} \sum_l P_l P_l + \frac{1}{2} k \sum_l (\eta_l \eta_l - \eta_l \eta_{l+1} - \eta_l \eta_{l-1}) \quad (17)$$

Here, M is the mass of each nucleus, k the elastic constant of the atomic bonds. P_l and η_l are the momentum and position operators, operating on a site indexed l . Harmonic approximation leads to neglecting terms beyond the first neighbor and assuming that k is identical between leftward and rightward neighbors. With these assumptions, one can show that this Hamiltonian in real space is equivalent to this one in momentum space [80]:

$$H = \frac{1}{2} \sum_q \left[\frac{1}{M} \Pi_q \Pi_q^* + 2k(1 - \cos q) \xi_q \xi_q^* \right] \quad (18)$$

The operators $\xi_q = \frac{1}{\sqrt{N}} \sum_l \eta_l s^{iql}$ and $\Pi_q = \frac{1}{\sqrt{N}} \sum_l P_l s^{-iql}$ are Fourier transforms of the single particle operators, allowing the coupled real space harmonic oscillators of Equation 17 to become independent reciprocal space oscillators of Equation 18. Hamiltonian 18 can be easily diagonalized. Its eigen-states are periodic: $|n_q\rangle \equiv |n_{q+2n\pi}\rangle$. Their projection in real space define one-dimensional phonons with a wave-vector and a frequency: $\langle x | n_q \rangle = e^{-i(qx - \omega t)}$.

As discussed in the previous section, in a finite magnetic field atomic displacements can acquire a BO phase ($\phi(x) = \frac{x\delta u}{\ell_B^2}$) and become $\langle x | n_q \rangle = e^{-i[(qx - \omega t) + \phi(x)]}$. Then, in a manner

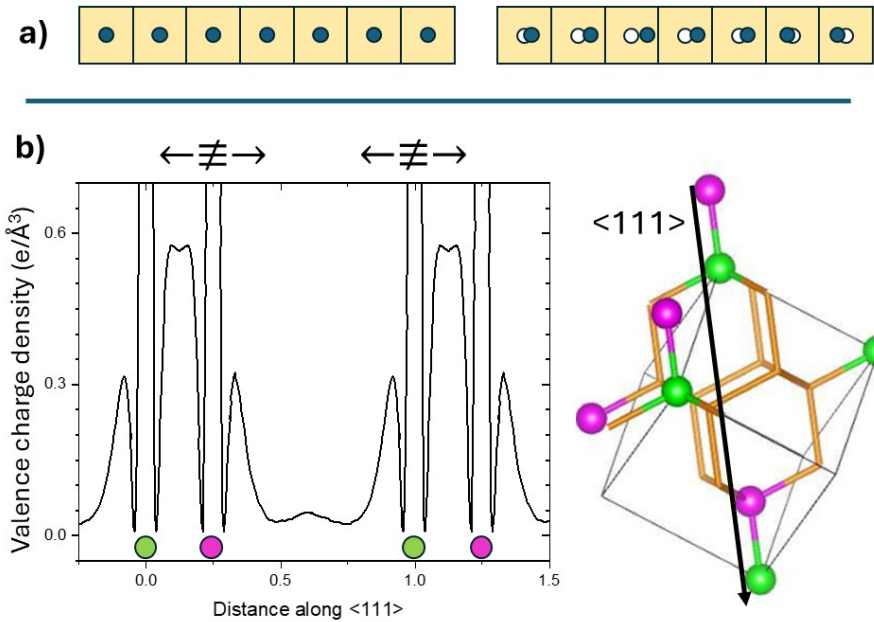


Figure 5: a) Left: A chain of centrosymmetric square unit cells containing an atom (dark blue circles) with electron cloud filling each unit cell. The overall phase is zero because there is no mismatch between the electronic and the nuclear center of mass. Right: A collective vibration of atoms leaving their equilibrium positions (white circles) would create a local mismatch between the nuclear and the electronic centers of mass. b) The computed valence charge density in silicon along the $<111>$ crystalline orientation [79]. The origin of the horizontal axis is an atomic site and the units are the body diagonal of the cube. The location of four atomic Si sites are represented by green and purple circles. For each atom, a displacements leftward and rightward are not equivalent. The right panel shows the unit cell of silicon. Only Si atoms corresponding to these two specific sites are shown.

similar to Bloch waves, one can proceed to their ‘Berryology’ [81]. The Berry connection is :

$$i \langle n_q | \nabla n_q \rangle = \frac{\delta \mathbf{u}}{\ell_B^2} \quad (19)$$

The Berry phase phase is obtained by integrating over a period:

$$\delta \phi_B = \lambda \overline{\frac{\delta \mathbf{u}}{\ell_B^2}} \quad (20)$$

In a harmonic approximation, the average atomic displacement, $\overline{\delta \mathbf{u}}$ is zero. Since leftward and rightward displacements contribute equally with opposite signs to the overall phase, the overall phase for a harmonic vibration of the atomic chain is zero. On the other hand, a difference between the amplitude of the atomic displacement at the crest and at the trough of the wave would lead to a finite Berry phase ($\propto \frac{\delta u_m \lambda_{ph}}{\ell_B^2}$).

Thus, anharmonicity is an indispensable ingredient for a finite phonon phase. The parameter q_e Equation 16 is a measure of this anharmonicity.

Real solids are anharmonic. Attraction and repulsion are asymmetric in the Lenard-Jones interaction. Figure 5b (taken from ref. [79]) shows the distribution of valence charge in silicon. Such non-trivial charge distribution, in this covalent insulator implies that leftward and rightward displacements of ions do not encounter the same restoring force.

As mentioned in section 3, the Grüneisen parameter [33] of a phonon mode i , defined by the logarithmic derivative of its frequency with respect to the volume: $\gamma_i = \frac{d\ln\omega_i}{d\ln V}$, is a widespread measure of anharmonicity. In silicon [82, 83], $\gamma \approx 1$ and this is not uncommon. Since the local lattice parameter is modified in the presence of a vibration, the significant distortion-induced frequency of phonons (i.e. γ_i) generates a large imbalance between atomic displacements at the crest and at the trough.

The elastic constants of a solid allow to write the free-energy density as a Taylor series in strain [84]:

$$\rho_0 E(\eta) = \rho_0 E(0) + \frac{1}{2!} \sum_{i,j=1}^6 C_{ij} \eta_i \eta_j + \frac{1}{3!} \sum_{i,j,k=1}^6 C_{ijk} \eta_i \eta_j \eta_k \quad (21)$$

Here ρ_0 is the mass density, and η is the strain tensor. C_{ij} and C_{ijk} are the second-order and the third-order elastic constants. The relative amplitude of the third order and the second order elastic constants sets the difference between imbalance between compressive and tensile strains. Neglecting anisotropy, one can write:

$$\left| \frac{\overline{\eta_{crest}} - \overline{\eta_{trough}}}{\overline{\eta}} \right| \simeq \frac{1}{3} \left| \frac{\overline{C_{ijk}}}{\overline{C_{ij}}} \right| \quad (22)$$

The elastic constants of silicon are extensively documented [85–87]. The second-order elastic constants are $C_{11}=165.64$, $C_{12}=63.94$, $C_{44}=79.51$ (in GPa). The third order elastic constants are significantly larger and mostly negative : $C_{111}=-795$, $C_{112}=-445$, $C_{123}=-75$, $C_{144}=15$, $C_{155}=-310$, $C_{444}=-86$ (all in GPa). As a consequence: $\frac{1}{3} \frac{\overline{C_{ijk}}}{\overline{C_{ij}}} \approx -1$. This indicates that at least in silicon, anharmonicity is large enough to expect $q_e \approx 1$.

Interestingly, in rare gas crystals with van der Waals binding, the available data [88] indicates that $\frac{1}{3} \frac{\overline{C_{ijk}}}{\overline{C_{ij}}} - 1$ holds in their case too. The Third-order elastic constants appear to exceed their second-order counterparts in most crystals. This appears to be driven by a significant third derivative ($\frac{d^3 V}{dr^3}$) of the potential energy regardless of the type of binding.

Even with a $q_e \approx 1$, the amplitude of $\delta\phi_B$ yielded by Equation 16 is small. When $B \approx 10$ T and $T \sim 10$ K, ℓ_B and λ_{ph} are comparable in magnitude (in the range of hundreds of angstroms) and δu_m is two to three orders of magnitude smaller. Therefore, in our range of interest the phonon phase is of the order of a few milli-radians, comparable to the phase shift of photons in a typical Kerr experiment on a magnetic material [89].

Such a phase can affect the interference between two phonons with different phases in the same magnetic field.

6 Normal collisions between complex phonons

Textbooks define phonons as quanta of lattice vibrations; waves of atomic displacements whose amplitude is a real vector. Complex waves have additional singularities [90] such as wavefront dislocations [91] where the wave vanishes because of its undefined phase. Let us now consider what can happen to sound waves acquiring a phase thanks to magnetic field.

Equation 6 can be revised by including $\delta\phi_B$, the phase difference between the original phonon and a second one, which by modifying the environment of the first, modulates its phase:

$$A = e^{i[\vec{q}_1 \cdot \vec{r} - \omega_1 t + C \cos(\vec{q}_2 \cdot \vec{r} - \omega_2 t + \delta\phi_B)]} \quad (23)$$

The Taylor expansion (Equation 8) becomes:

$$\begin{aligned} A \simeq e^{i(\vec{q}_1 \cdot \vec{r} - \omega_1 t)} \\ + \frac{1}{2} C i e^{i[(\vec{q}_1 + \vec{q}_2) \cdot \vec{r} - (\omega_1 + \omega_2)t + \delta\phi_B]} \\ + \frac{1}{2} C i e^{i[(\vec{q}_1 - \vec{q}_2) \cdot \vec{r} - (\omega_1 - \omega_2)t] - \delta\phi_B} \end{aligned} \quad (24)$$

Comparing equation 24 with equation 9, one can detect a difference. Now there is a $e^{2i\delta\phi_B}$ difference between the prefactors of absorption and emission events. The difference between the amplitude of the absorption and emission waves opens the road for a thermal Hall response. Let us call the angle between \vec{q}_1 and \vec{q}_2 , θ , and the component of \vec{q}_3 , perpendicular to \vec{q}_1 , $q_{3\perp}$. Then it is easy to see that for an absorption event, $q_{3\perp} = q_2 \sin \theta$ and for an emission event, $q_{3\perp} = -q_2 \sin \theta$. For both emission and absorption events, the final wave-vector (\vec{q}_3) becomes tilted with respect to the original wavevector (\vec{q}_1). Since the sign of the perpendicular wavevectors $q_{3\perp}$ is opposite for emission and absorption, the net tilt is zero when both types of events weigh equally.

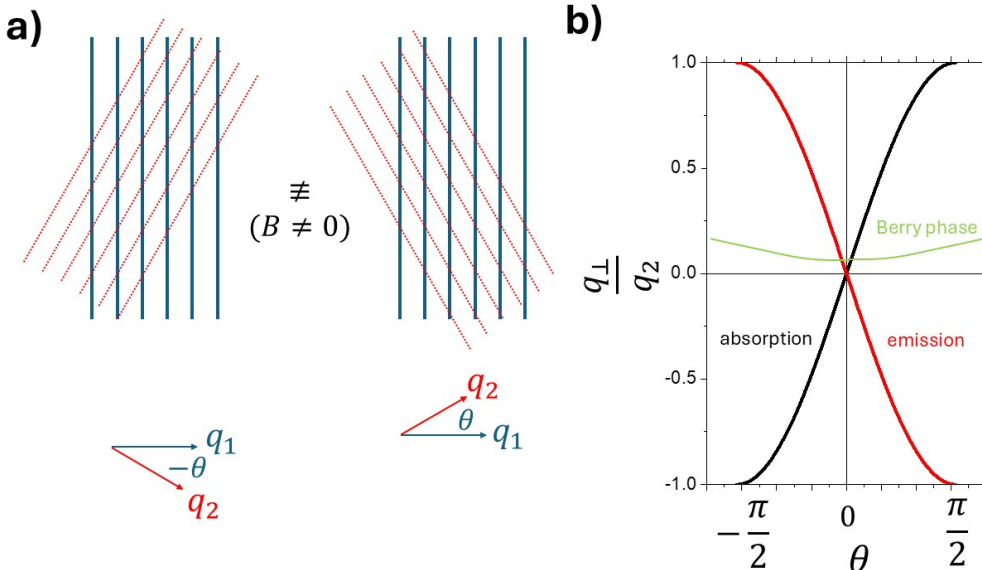


Figure 6: a) An illustration of interference between two lattice waves. In the absence of magnetic field, the two configurations are equivalent but not in its presence. b) The normalized amplitude of the perpendicular wave-vectors produced by absorption and emission events. In absence of a finite Berry phase, they would cancel each other, but not in its presence.

Consider a phonon with a \vec{q}_1 wave-vector traveling in an isotropic plane and encountering another phonon with a wavevector \vec{q}_2 . In absence of a magnetic field, there is no difference if the angle between \vec{q}_1 and \vec{q}_2 is θ or $-\theta$. This would not happen in the presence of a finite

$\delta\phi_B$. Even at $\theta = 0$, the latter can be finite. This is sufficient to generate a Hall signal (See Figure 6).

7 Comparison between the expected and the observed amplitudes of the thermal Hall angle

The simple picture drawn above can provide answers to two questions raised by experiments. Why does the thermal Hall angle peak at T_{max} ? Because this is where the Normal phonon-phonon scattering is most prominent. How can the magnetic field induce heat flow without entropy production? By inducing a phase, which modifies Normal phonon-phonon wave interference.

What about the amplitude of the thermal Hall signal?

A rigorous answer to this question is a task for *ab initio* studies starting from the phonon spectrum in each solid. In 2019, Saito and collaborators [43] proposed that in a nonmagnetic insulator with ordinary phonons, such as silicon, Berry phase can give rise to a detectable thermal Hall effect. Their expected thermal hall conductivity at room temperature was $10^{-6} \text{ WK}^{-1} \text{ m}^{-1}$. As seen in table 1, the experimentally observed thermal Hall conductivity in silicon [15] is 7 orders of magnitude larger! Anharmonicity, the central player in our scenario, was not mentioned there [43]. The amplitude of the thermal Hall conductivity correlates with the maximum longitudinal thermal conductivity. The latter is known to depend on the sample size [62]. The maximum thermal conductivity is not an intrinsic property. In silicon crystals [92] larger than the one in which the thermal Hall conductivity was measured [15], longitudinal thermal conductivity is several times larger.

In the picture drawn here, the Hall angle, the ratio of longitudinal to transverse thermal conductivities at T_{max} (see table 1), is the central quantity to put under scrutiny. If the field-induced misalignment between the heat current and the temperature gradient is due to interference between phonons, then one expects it to be bounded by $\approx 2\delta\phi_B$.

Solid	T_D (K)	T_{max} (K)	$\kappa_{ii}(\text{WK}^{-1} \text{ m}^{-1})$	$\kappa_{ij}(\text{WK}^{-1} \text{ m}^{-1})$	$\frac{\kappa_{ij}}{\kappa_{ii}} B^{-1} (10^{-4} \text{ T}^{-1})$
Si	636	33	1880	10.6 (9 T)	6.3
Ge	363	20	610	2.5 (9 T)	4.6
Black P	306	24	1900-300	2 (12T)	0.9-5.5

Table 1: Longitudinal and transverse thermal conductivity in silicon [15], germanium [15] and black phosphorous [12]. T_D is the Debye temperature [62, 93] and T_{max} the temperature at which both the longitudinal (κ_{ii}) and the transverse (κ_{ij}) thermal conductivity peak. The next two columns list their amplitudes at T_{max} . In black phosphorus, the two values for κ_{ii} correspond to two different crystalline orientations [12, 62]. The last column represents the Hall angle normalized by the magnetic field.

Quantifying λ_{ph} and δu_m at T_{max} in the three elemental insulators listed in table 1 would allow a comparison between the experimental data and the picture drawn here.

An acoustic phonon with linear dispersion has a velocity of $v_{ph} = \omega/q$. Since the wavevector ($q = \frac{2\pi}{\lambda_{ph}}$) is simply proportional to thermal energy, the wavelength is proportional to the inverse of temperature. At, $T = T_{max}$, it becomes :

$$\lambda_{ph}(T_{max}) \approx \frac{\hbar v_{ph}}{k_B T_{max}} \quad (25)$$

Solid	Mass (a.u.)	a (Å)	v_{ph} (km/s)	$\lambda_{ph}(T_{max})$ (Å)	$\delta u_m(T_{max})$ (Å)	$\lambda_{ph} \delta u_m \frac{e}{\hbar} (10^{-4} T^{-1})$
Si	28.1	2.72	9.0	130	0.23	4.6
Ge	72.6	2.83	5.9	141	0.18	3.9
Black P	31	2.74	3-8.5	60-170	0.25	2.2-6.5

Table 2: Atomic masses and length scales of silicon, germanium and phosphorous. $a = (V_c/n_c)^{1/3}$ is the average distance per atoms (with V_c and n_c are the volume of the primitive cell and its number of atoms). v_{ph} is the longitudinal sound velocity used to extract the phonon wavelength at $T=T_{max}$. The two values for Black P represent the lowest and the largest [62]. δu_m , the crest atomic displacement at $T=T_{max}$ was extracted from Equation 26. The last column is to be compared with the last column of table 1.

At $T=0$, q vanishes and the wavelength of a thermally excited phonon becomes infinite. This of course never happens in a solid of finite size. In realistic experimental set-ups, we are far from this limit. Given that sound velocity in solids is between 1 to 20 km/s, the wavelength of thermally excited phonons is about in the range of ~ 10 nm at 1 K and $\sim 1\mu$ m at 10 mK. The samples studied in these experiments are much larger than these length scales.

The amplitude of δu_m , the atomic displacement at the crest of a lattice wave is linked to the energy of the thermally excited phonon mode: $M \delta u_m^2 \omega_{ph}^2 = k_B T_{max}$, where M is the atomic mass [94]. Combined with $\hbar \omega_{ph}(T_{max}) = k_B T_{max}$, it becomes:

$$\delta u_m(T_{max}) \approx \frac{\hbar}{\sqrt{M k_B T_{max}}} \quad (26)$$

Thus, δu_m is proportional to the de Broglie thermal length of the vibrating atom and diverges at $T=0$. This divergence is weaker than the zero-temperature divergence of $\lambda_{ph}(T)$. In our temperature range of interest, δu_m remains shorter than the interatomic distance, a (See table 2).

Table 2 lists the established values for the three solids. For cubic silicon and germanium, extracting them from equations 25 and 26 is straightforward. Orthorhombic black P is significantly anisotropic. Remarkably, the last columns in table 1 and in table 2) are comparable. If an upper bound to the amplitude of the thermal Hall angle is set by Equation 16 and if $q_e \approx 1$, then this observation ceases to be surprising.

8 Concluding remarks

We started from two experimental observation: i) The Hall angle peaks at the peak temperature of longitudinal thermal conductivity; ii) The amplitude of this peak thermal angle is similar in different insulators. This led us to the implications of a finite thermal Hall angle in section 2. Its finite value implies flow of heat without entropy production. In section 3, we saw that the frequency of Normal phonon-phonon scattering events, which do not produce entropy, is most prominent at the peak temperature of longitudinal thermal conductivity. Such collisions are therefore suspected to play a role. Section 4 recalled that in the Born-Oppenheimer approximation, magnetic field gives rise to phase to the atomic and the molecular wavefunctions. Section 5 argued that combination of this phase and anharmonicity yields a geometric (Berry) phase to acoustic phonons in a magnetic field. The consequences of the Berry phase for Normal events were discussed in Section 6. Because of this phase, magnetic field becomes

a ‘ratchet’ creating an imbalance between absorption and emission Normal events. Finally, in section 7, the rough magnitude of the expected peak signal was found to match what has been experimentally observed.

In his ‘Notes subject to ongoing editing’ Resta [41] (circa 2022) commented that “The general problem of the nuclear motion—both classical and quantum—in presence of an external magnetic field has been first solved in 1988 by Schmelcher, Cederbaum, and Meyer [35]. It is remarkable that such a fundamental problem was solved so late, and that even today the relevant literature is ignored by textbooks and little cited.”

To this very pertinent judgment, one may add that it is also remarkable that their consequences for phonons have not been examined. If the phase of the wavefunction matters for molecules, why should it be neglected for a sound wave in a crystal ?

Inspired by Mead’s treatment of molecules [37], it appears appropriate to call the present scenario the ‘lattice Aharonov-Bohm effect’. Note that, like the ‘molecular Aharonov-Bohm effect’ [95, 96], as well as the Berry phase [97], it is about a geometric (and not a topological) phase.

9 Acknowledgments

The author thanks Benoît Fauqué, Xiaokang Li, Arthur Marguerite and Zengwei Zhu for helpful discussions.

References

- [1] C. Strohm, G. L. J. A. Rikken and P. Wyder, *Phenomenological evidence for the phonon Hall effect*, Phys. Rev. Lett. **95**, 155901 (2005), doi:[10.1103/PhysRevLett.95.155901](https://doi.org/10.1103/PhysRevLett.95.155901).
- [2] K. Sugii, M. Shimozawa, D. Watanabe, Y. Suzuki, M. Halim, M. Kimata, Y. Matsumoto, S. Nakatsuji and M. Yamashita, *Thermal Hall effect in a phonon-glass $\text{Ba}_3\text{CuSb}_2\text{O}_9$* , Phys. Rev. Lett. **118**, 145902 (2017), doi:[10.1103/PhysRevLett.118.145902](https://doi.org/10.1103/PhysRevLett.118.145902).
- [3] Y. Hirokane, Y. Nii, Y. Tomioka and Y. Onose, *Phononic thermal Hall effect in diluted terbium oxides*, Phys. Rev. B **99**, 134419 (2019), doi:[10.1103/PhysRevB.99.134419](https://doi.org/10.1103/PhysRevB.99.134419).
- [4] X. Li, B. Fauqué, Z. Zhu and K. Behnia, *Phonon thermal Hall effect in strontium titanate*, Phys. Rev. Lett. **124**, 105901 (2020), doi:[10.1103/PhysRevLett.124.105901](https://doi.org/10.1103/PhysRevLett.124.105901).
- [5] G. Grissonnanche, S. Thériault, A. Gourgout, M.-E. Boulanger, E. Lefrançois, A. Ataei, F. Laliberté, M. Dion, J.-S. Zhou, S. Pyon *et al.*, *Chiral phonons in the pseudogap phase of cuprates*, Nature Physics **16**(11), 1108 (2020), doi:[10.1038/s41567-020-0965-y](https://doi.org/10.1038/s41567-020-0965-y).
- [6] M.-E. Boulanger, G. Grissonnanche, S. Badoux, A. Allaire, É. Lefrançois, A. Legros, A. Gourgout, M. Dion, C. Wang, X. Chen *et al.*, *Thermal Hall conductivity in the cuprate mott insulators Nd_2CuO_4 and $\text{Sr}_2\text{CuO}_2\text{Cl}_2$* , Nature Communications **11**(5325), 1 (2020), doi:[10.1038/s41467-020-18881-z](https://doi.org/10.1038/s41467-020-18881-z).
- [7] M. Akazawa, M. Shimozawa, S. Kittaka, T. Sakakibara, R. Okuma, Z. Hiroi, H.-Y. Lee, N. Kawashima, J. H. Han and M. Yamashita, *Thermal Hall effects of spins and phonons in kagome antiferromagnet Cd-Kapellasite*, Phys. Rev. X **10**, 041059 (2020), doi:[10.1103/PhysRevX.10.041059](https://doi.org/10.1103/PhysRevX.10.041059).

[8] L. Chen, M.-E. Boulanger, Z.-C. Wang, F. Tafti and L. Taillefer, *Large phonon thermal Hall conductivity in the antiferromagnetic insulator Cu₃TeO₆*, Proceedings of the National Academy of Sciences **119**(34), e2208016119 (2022), doi:[10.1073/pnas.2208016119](https://doi.org/10.1073/pnas.2208016119).

[9] T. Uehara, T. Ohtsuki, M. Udagawa, S. Nakatsuji and Y. Machida, *Phonon thermal Hall effect in a metallic spin ice*, Nature Communications **13**(4604), 1 (2022), doi:[10.1038/s41467-022-32375-0](https://doi.org/10.1038/s41467-022-32375-0).

[10] S. Jiang, X. Li, B. Fauqué and K. Behnia, *Phonon drag thermal Hall effect in metallic strontium titanate*, Proceedings of the National Academy of Sciences **119**(35), e2201975119 (2022), doi:[10.1073/pnas.2201975119](https://doi.org/10.1073/pnas.2201975119).

[11] E. Lefrançois, G. Grissonnanche, J. Baglo, P. Lampen-Kelley, J.-Q. Yan, C. Balz, D. Mandrus, S. E. Nagler, S. Kim, Y.-J. Kim, N. Doiron-Leyraud and L. Taillefer, *Evidence of a phonon Hall effect in the Kitaev spin liquid candidate α -RuCl₃*, Phys. Rev. X **12**, 021025 (2022), doi:[10.1103/PhysRevX.12.021025](https://doi.org/10.1103/PhysRevX.12.021025).

[12] X. Li, Y. Machida, A. Subedi, Z. Zhu, L. Li and K. Behnia, *The phonon thermal Hall angle in black phosphorus*, Nature Communications **14**(1), 1027 (2023), doi:[10.1038/s41467-023-36750-3](https://doi.org/10.1038/s41467-023-36750-3).

[13] R. Sharma, M. Bagchi, Y. Wang, Y. Ando and T. Lorenz, *Phonon thermal Hall effect in charge-compensated topological insulators*, Phys. Rev. B **109**, 104304 (2024), doi:[10.1103/PhysRevB.109.104304](https://doi.org/10.1103/PhysRevB.109.104304).

[14] Q. Meng, X. Li, L. Zhao, C. Dong, Z. Zhu and K. Behnia, *Thermodynamic origin of the phonon Hall effect in a honeycomb antiferromagnet* (2024), [2403.13306](https://arxiv.org/abs/2403.13306).

[15] X. Jin, X. Zhang, W. Wan, H. Wang, Y. Jiao and S. Li, *Discovery of universal phonon thermal Hall effect in crystals*, arXiv preprint arXiv:2404.02863 (2024).

[16] A. Vallipuram, L. Chen, E. Campillo, M. Mezidi, G. Grissonnanche, M.-E. Boulanger, E. Lefrançois, M. P. Zic, Y. Li, I. R. Fisher, J. Baglo and L. Taillefer, *Role of magnetic ions in the thermal Hall effect of the paramagnetic insulator TmVO₄*, Phys. Rev. B **110**, 045144 (2024), doi:[10.1103/PhysRevB.110.045144](https://doi.org/10.1103/PhysRevB.110.045144).

[17] L. Chen, É. Lefrançois, A. Vallipuram, Q. Barthélémy, A. Ataei, W. Yao, Y. Li and L. Taillefer, *Planar thermal Hall effect from phonons in a kitaev candidate material*, Nature Communications **15**(1), 3513 (2024), doi:[10.1038/s41467-024-47858-5](https://doi.org/10.1038/s41467-024-47858-5).

[18] L. Sheng, D. N. Sheng and C. S. Ting, *Theory of the phonon Hall effect in paramagnetic dielectrics*, Phys. Rev. Lett. **96**, 155901 (2006), doi:[10.1103/PhysRevLett.96.155901](https://doi.org/10.1103/PhysRevLett.96.155901).

[19] Y. Kagan and L. A. Maksimov, *Anomalous Hall effect for the phonon heat conductivity in paramagnetic dielectrics*, Phys. Rev. Lett. **100**, 145902 (2008), doi:[10.1103/PhysRevLett.100.145902](https://doi.org/10.1103/PhysRevLett.100.145902).

[20] L. Zhang, J. Ren, J.-S. Wang and B. Li, *Topological nature of the phonon Hall effect*, Phys. Rev. Lett. **105**, 225901 (2010), doi:[10.1103/PhysRevLett.105.225901](https://doi.org/10.1103/PhysRevLett.105.225901).

[21] T. Qin, J. Zhou and J. Shi, *Berry curvature and the phonon Hall effect*, Phys. Rev. B **86**, 104305 (2012), doi:[10.1103/PhysRevB.86.104305](https://doi.org/10.1103/PhysRevB.86.104305).

[22] B. K. Agarwalla, L. Zhang, J.-S. Wang and B. Li, *Phonon Hall effect in ionic crystals in the presence of static magnetic field*, The European Physical Journal B **81**(2), 197 (2011), doi:[10.1140/epjb/e2011-11002-x](https://doi.org/10.1140/epjb/e2011-11002-x).

[23] J.-Y. Chen, S. A. Kivelson and X.-Q. Sun, *Enhanced thermal Hall effect in nearly ferroelectric insulators*, Phys. Rev. Lett. **124**, 167601 (2020), doi:[10.1103/PhysRevLett.124.167601](https://doi.org/10.1103/PhysRevLett.124.167601).

[24] B. Flebus and A. H. MacDonald, *Charged defects and phonon Hall effects in ionic crystals*, Phys. Rev. B **105**, L220301 (2022), doi:[10.1103/PhysRevB.105.L220301](https://doi.org/10.1103/PhysRevB.105.L220301).

[25] H. Guo, D. G. Joshi and S. Sachdev, *Resonant thermal Hall effect of phonons coupled to dynamical defects*, Proceedings of the National Academy of Sciences **119**(46), e2215141119 (2022), doi:[10.1073/pnas.2215141119](https://doi.org/10.1073/pnas.2215141119).

[26] L. Mangeolle, L. Balents and L. Savary, *Phonon thermal Hall conductivity from scattering with collective fluctuations*, Phys. Rev. X **12**, 041031 (2022), doi:[10.1103/PhysRevX.12.041031](https://doi.org/10.1103/PhysRevX.12.041031).

[27] L. Zhang and Q. Niu, *Angular momentum of phonons and the Einstein-de Haas effect*, Phys. Rev. Lett. **112**, 085503 (2014), doi:[10.1103/PhysRevLett.112.085503](https://doi.org/10.1103/PhysRevLett.112.085503).

[28] D. M. Juraschek and N. A. Spaldin, *Orbital magnetic moments of phonons*, Phys. Rev. Mater. **3**, 064405 (2019), doi:[10.1103/PhysRevMaterials.3.064405](https://doi.org/10.1103/PhysRevMaterials.3.064405).

[29] X. Dai, *Large thermal Hall effect detected in elemental covalent insulators*, Journal Club for Condensed Matter Physics (2024), doi:[10.36471/JCCM_October_2024_02](https://doi.org/10.36471/JCCM_October_2024_02).

[30] L. Lindsay, D. A. Broido and T. L. Reinecke, *Ab initio thermal transport in compound semiconductors*, Phys. Rev. B **87**, 165201 (2013), doi:[10.1103/PhysRevB.87.165201](https://doi.org/10.1103/PhysRevB.87.165201).

[31] R. Berman, *Thermal Conduction in Solids*, Oxford studies in physics. Clarendon Press (1976).

[32] J. W. Vandersande and C. Wood, *The thermal conductivity of insulators and semiconductors*, Contemporary Physics **27**(2), 117 (1986), doi:[10.1080/00107518608211003](https://doi.org/10.1080/00107518608211003).

[33] N. W. Ashcroft and N. D. Mermin, *Solid State Physics*, Holt-Saunders (1976).

[34] M. Born and R. Oppenheimer, *Zur quantentheorie der moleküle*, Annalen der Physik **389**(20), 457 (1927), doi:<https://doi.org/10.1002/andp.19273892002>, <https://onlinelibrary.wiley.com/doi/10.1002/andp.19273892002>.

[35] P. Schmelcher, L. S. Cederbaum and H.-D. Meyer, *Electronic and nuclear motion and their couplings in the presence of a magnetic field*, Phys. Rev. A **38**, 6066 (1988), doi:[10.1103/PhysRevA.38.6066](https://doi.org/10.1103/PhysRevA.38.6066).

[36] P. Schmelcher, L. S. Cederbaum and H. D. Meyer, *On the validity of the Born-Oppenheimer approximation in magnetic fields*, Journal of Physics B: Atomic, Molecular and Optical Physics **21**(15), L445 (1988), doi:[10.1088/0953-4075/21/15/005](https://doi.org/10.1088/0953-4075/21/15/005).

[37] C. Alden Mead, *The molecular Aharonov—Bohm effect in bound states*, Chemical Physics **49**(1), 23 (1980), doi:[https://doi.org/10.1016/0301-0104\(80\)85035-X](https://doi.org/10.1016/0301-0104(80)85035-X).

[38] C. A. Mead, *The geometric phase in molecular systems*, Rev. Mod. Phys. **64**, 51 (1992), doi:[10.1103/RevModPhys.64.51](https://doi.org/10.1103/RevModPhys.64.51).

[39] M. V. Berry, R. G. Chambers, M. D. Large, C. Upstill and J. C. Walmsley, *Wavefront dislocations in the aharonov-bohm effect and its water wave analogue*, European Journal of Physics **1**(3), 154 (1980), doi:[10.1088/0143-0807/1/3/008](https://doi.org/10.1088/0143-0807/1/3/008).

[40] R. Resta, *Manifestations of Berry's phase in molecules and condensed matter*, Journal of Physics: Condensed Matter **12**(9), R107 (2000), doi:[10.1088/0953-8984/12/9/201](https://doi.org/10.1088/0953-8984/12/9/201).

[41] R. Resta, *Geometry and topology in electronic structure theory, Lecture notes available on University of Trieste website* (2022).

[42] A. Bohm, A. Mostafazadeh, H. Koizumi, Q. Niu and J. Zwanziger, *The Geometric phase in quantum systems: foundations, mathematical concepts, and applications in molecular and condensed matter physics*, Springer Science & Business Media (2013).

[43] T. Saito, K. Misaki, H. Ishizuka and N. Nagaosa, *Berry phase of phonons and thermal hall effect in nonmagnetic insulators*, Phys. Rev. Lett. **123**, 255901 (2019), doi:[10.1103/PhysRevLett.123.255901](https://doi.org/10.1103/PhysRevLett.123.255901).

[44] X. Li, X. Guo, Z. Zhu and K. Behnia, *Angle-dependent planar thermal hall effect by quasi-ballistic phonons in black phosphorus*, Science Bulletin **70**(12), 1962 (2025), doi:<https://doi.org/10.1016/j.scib.2025.03.052>.

[45] R. P. Feynman, R. B. Leighton and M. Sands, *The Feynman lectures on physics; New millennium ed.*, Basic Books, New York, NY, Originally published 1963-1965 (2010).

[46] S. de Groot and P. Mazur, *Non-equilibrium Thermodynamics*, Dover Books on Physics. Dover Publications, ISBN 9780486647418 (1984).

[47] D. Jou and G. Lebon, *Extended Irreversible Thermodynamics*, Springer Dordrecht, doi:[10.1007/978-90-481-3074-0](https://doi.org/10.1007/978-90-481-3074-0) (2010).

[48] P. Hänggi, F. Marchesoni and F. Nori, *Brownian motors*, Annalen der Physik **517**(1-3), 51 (2005), doi:<https://doi.org/10.1002/andp.200551701-304>.

[49] P. Reimann, *Brownian motors: noisy transport far from equilibrium*, Physics Reports **361**(2), 57 (2002), doi:[https://doi.org/10.1016/S0370-1573\(01\)00081-3](https://doi.org/10.1016/S0370-1573(01)00081-3).

[50] C. Van den Broeck, R. Kawai and P. Meurs, *Microscopic analysis of a thermal brownian motor*, Phys. Rev. Lett. **93**, 090601 (2004), doi:[10.1103/PhysRevLett.93.090601](https://doi.org/10.1103/PhysRevLett.93.090601).

[51] J. M. R. Parrondo and P. Español, *Criticism of Feynman's analysis of the ratchet as an engine*, American Journal of Physics **64**(9), 1125 (1996), doi:[10.1119/1.18393](https://doi.org/10.1119/1.18393).

[52] S. P. Łepkowski, *First-principles calculation of higher-order elastic constants using exact deformation-gradient tensors*, Phys. Rev. B **102**, 134116 (2020), doi:[10.1103/PhysRevB.102.134116](https://doi.org/10.1103/PhysRevB.102.134116).

[53] T. Middelmann, A. Walkov, G. Bartl and R. Schödel, *Thermal expansion coefficient of single-crystal silicon from 7 k to 293 k*, Phys. Rev. B **92**, 174113 (2015), doi:[10.1103/PhysRevB.92.174113](https://doi.org/10.1103/PhysRevB.92.174113).

[54] D. S. Kim, O. Hellman, J. Herriman, H. L. Smith, J. Y. Y. Lin, N. Shulumba, J. L. Niedziela, C. W. Li, D. L. Abernathy and B. Fultz, *Nuclear quantum effect with pure anharmonicity and the anomalous thermal expansion of silicon*, Proceedings of the National Academy of Sciences **115**(9), 1992 (2018), doi:[10.1073/pnas.1707745115](https://doi.org/10.1073/pnas.1707745115).

[55] J. Hook and H. Hall, *Solid State Physics*, Manchester Physics Series. Wiley, ISBN 9781118790885 (2013).

[56] T. Feng, L. Lindsay and X. Ruan, *Four-phonon scattering significantly reduces intrinsic thermal conductivity of solids*, Phys. Rev. B **96**, 161201 (2017), doi:[10.1103/PhysRevB.96.161201](https://doi.org/10.1103/PhysRevB.96.161201).

[57] A. A. Maznev and O. B. Wright, *Demystifying umklapp vs normal scattering in lattice thermal conductivity*, American Journal of Physics **82**(11), 1062 (2014), doi:[10.1119/1.4892612](https://doi.org/10.1119/1.4892612).

[58] R. A. Guyer and J. A. Krumhansl, *Thermal conductivity, second sound, and phonon hydrodynamic phenomena in nonmetallic crystals*, Phys. Rev. **148**, 778 (1966).

[59] H. Beck, P. F. Meier and A. Thellung, *Phonon hydrodynamics in solids*, physica status solidi (a) **24**(1), 11 (1974).

[60] A. Cepellotti, G. Fugallo, L. Paulatto, M. Lazzeri, F. Mauri and N. Marzari, *Phonon hydrodynamics in two-dimensional materials*, Nat. Commun. **6**(1), 6400 (2015).

[61] V. Martelli, J. L. Jiménez, M. Continentino, E. Baggio-Saitovitch and K. Behnia, *Thermal transport and phonon hydrodynamics in strontium titanate*, Phys. Rev. Lett. **120**, 125901 (2018), doi:[10.1103/PhysRevLett.120.125901](https://doi.org/10.1103/PhysRevLett.120.125901).

[62] Y. Machida, A. Subedi, K. Akiba, A. Miyake, M. Tokunaga, Y. Akahama, K. Izawa and K. Behnia, *Observation of poiseuille flow of phonons in black phosphorus*, Science Advances **4**(6), eaat3374 (2018), doi:[10.1126/sciadv.aat3374](https://doi.org/10.1126/sciadv.aat3374).

[63] Y. Machida, N. Matsumoto, T. Isono and K. Behnia, *Phonon hydrodynamics and ultra-high-room temperature thermal conductivity in thin graphite*, Science **367**, 309 (2020).

[64] K. Ghosh, A. Kusiak and J.-L. Battaglia, *Phonon hydrodynamics in crystalline materials*, Journal of Physics: Condensed Matter **34**(32), 323001 (2022), doi:[10.1088/1361-648X/ac718a](https://doi.org/10.1088/1361-648X/ac718a).

[65] A. Jaoui, A. Gourgout, G. Seyfarth, A. Subedi, T. Lorenz, B. Fauqué and K. Behnia, *Formation of an electron-phonon bifluid in bulk antimony*, Phys. Rev. X **12**, 031023 (2022), doi:[10.1103/PhysRevX.12.031023](https://doi.org/10.1103/PhysRevX.12.031023).

[66] Y. Machida, V. Martelli, A. Jaoui, B. Fauqué and K. Behnia, *Phonon hydrodynamics in bulk insulators and semimetals*, Low Temp. Phys. **50**(7), 574 (2024), doi:[10.1063/10.0026323](https://doi.org/10.1063/10.0026323).

[67] T. Kawabata, K. Shimura, Y. Ishii, M. Koike, K. Yoshida, S. Yonehara, K. Yokoi, A. Subedi, K. Behnia and Y. Machida, *Phonon hydrodynamic regimes in sapphire* (2024), **2407.16196**.

[68] L. S. Cederbaum, *The exact molecular wavefunction as a product of an electronic and a nuclear wavefunction*, The Journal of Chemical Physics **138**(22), 224110 (2013), doi:[10.1063/1.4807115](https://doi.org/10.1063/1.4807115).

[69] F. G. Eich and F. Agostini, *The adiabatic limit of the exact factorization of the electron-nuclear wave function*, The Journal of Chemical Physics **145**(5), 054110 (2016), doi:[10.1063/1.4959962](https://doi.org/10.1063/1.4959962), https://pubs.aip.org/aip/jcp/article-pdf/doi/10.1063/1.4959962/15515824/054110_1_online.pdf.

[70] P. B. Allen, *Anharmonic phonon quasiparticle theory of zero-point and thermal shifts in insulators: Heat capacity, bulk modulus, and thermal expansion*, Phys. Rev. B **92**, 064106 (2015), doi:[10.1103/PhysRevB.92.064106](https://doi.org/10.1103/PhysRevB.92.064106).

[71] G. A. Worth and L. S. Cederbaum, *Beyond Born-Oppenheimer: Molecular dynamics through a conical intersection*, Annual Review of Physical Chemistry **55**, 127 (2004), doi:<https://doi.org/10.1146/annurev.physchem.55.091602.094335>.

[72] I. Bersuker, *The Jahn-Teller Effect*, p. 12–44, Cambridge University Press (2006).

[73] C. A. Mead and D. G. Truhlar, *On the determination of Born–Oppenheimer nuclear motion wave functions including complications due to conical intersections and identical nuclei*, The Journal of Chemical Physics **70**(5), 2284 (1979), doi:[10.1063/1.437734](https://doi.org/10.1063/1.437734), https://pubs.aip.org/aip/jcp/article-pdf/70/5/2284/18916340/2284_1_online.pdf.

[74] H. C. Longuet-Higgins, U. Öpik, M. H. L. Pryce and R. A. Sack, *Studies of the Jahn-Teller effect .ii. the dynamical problem*, Proceedings of the Royal Society of London. Series A. Mathematical and Physical Sciences **244**(1236), 1 (1958), doi:[10.1098/rspa.1958.0022](https://doi.org/10.1098/rspa.1958.0022), <https://royalsocietypublishing.org/doi/pdf/10.1098/rspa.1958.0022>.

[75] Y. Aharonov and D. Bohm, *Significance of electromagnetic potentials in the quantum theory*, Phys. Rev. **115**, 485 (1959), doi:[10.1103/PhysRev.115.485](https://doi.org/10.1103/PhysRev.115.485).

[76] T. Culpitt, L. D. M. Peters, E. I. Tellgren and T. Helgaker, *Ab initio molecular dynamics with screened lorentz forces. i. calculation and atomic charge interpretation of berry curvature*, The Journal of Chemical Physics **155**(2), 024104 (2021), doi:[10.1063/5.0055388](https://doi.org/10.1063/5.0055388), https://pubs.aip.org/aip/jcp/article-pdf/doi/10.1063/5.0055388/16072098/024104_1_online.pdf.

[77] L. D. M. Peters, T. Culpitt, L. Monzel, E. I. Tellgren and T. Helgaker, *Ab initio molecular dynamics with screened lorentz forces. ii. efficient propagators and rovibrational spectra in strong magnetic fields*, The Journal of Chemical Physics **155**(2), 024105 (2021), doi:[10.1063/5.0056235](https://doi.org/10.1063/5.0056235), https://pubs.aip.org/aip/jcp/article-pdf/doi/10.1063/5.0056235/16071915/024105_1_online.pdf.

[78] T. Culpitt, E. I. Tellgren, L. D. M. Peters and T. Helgaker, *Non-adiabatic coupling matrix elements in a magnetic field: Geometric gauge dependence and Berry phase*, The Journal of Chemical Physics **161**(18), 184109 (2024), doi:[10.1063/5.0229854](https://doi.org/10.1063/5.0229854).

[79] Z. W. Lu, A. Zunger and M. Deutsch, *Electronic charge distribution in crystalline diamond, silicon, and germanium*, Phys. Rev. B **47**, 9385 (1993), doi:[10.1103/PhysRevB.47.9385](https://doi.org/10.1103/PhysRevB.47.9385).

[80] J. M. Ziman, *Electrons and Phonons: The Theory of Transport Phenomena in Solids*, International series of monographs on physics. OUP Oxford (2001).

[81] D. Gosálbez-Martínez, I. Souza and D. Vanderbilt, *Chiral degeneracies and fermi-surface chern numbers in bcc Fe*, Phys. Rev. B **92**, 085138 (2015), doi:[10.1103/PhysRevB.92.085138](https://doi.org/10.1103/PhysRevB.92.085138).

[82] T. Soma, H. Matsuo and Y. Saitoh, *Volume-dependence of phonon frequencies and mode grüneisen parameters for si and ge*, Solid State Communications **39**(11), 1193 (1981), doi:[https://doi.org/10.1016/0038-1098\(81\)91112-1](https://doi.org/10.1016/0038-1098(81)91112-1).

[83] D. A. Broido, A. Ward and N. Mingo, *Lattice thermal conductivity of silicon from empirical interatomic potentials*, Phys. Rev. B **72**, 014308 (2005), doi:[10.1103/PhysRevB.72.014308](https://doi.org/10.1103/PhysRevB.72.014308).

[84] S. P. Łepkowski, *First-principles calculation of higher-order elastic constants using exact deformation-gradient tensors*, Phys. Rev. B **102**, 134116 (2020), doi:[10.1103/PhysRevB.102.134116](https://doi.org/10.1103/PhysRevB.102.134116).

[85] P. N. Keating, *Theory of the third-order elastic constants of diamond-like crystals*, Phys. Rev. **149**, 674 (1966), doi:[10.1103/PhysRev.149.674](https://doi.org/10.1103/PhysRev.149.674).

[86] J. J. Hall, *Electronic effects in the elastic constants of n -type silicon*, Phys. Rev. **161**, 756 (1967), doi:[10.1103/PhysRev.161.756](https://doi.org/10.1103/PhysRev.161.756).

[87] J. Zhao, J. M. Winey and Y. M. Gupta, *First-principles calculations of second- and third-order elastic constants for single crystals of arbitrary symmetry*, Phys. Rev. B **75**, 094105 (2007), doi:[10.1103/PhysRevB.75.094105](https://doi.org/10.1103/PhysRevB.75.094105).

[88] I. J. Zucker and D. Paik, *Three-body forces and the third-order elastic constants of the rare gas crystals*, Journal of Physics C: Solid State Physics **12**(5), 771 (1979), doi:[10.1088/0022-3719/12/5/009](https://doi.org/10.1088/0022-3719/12/5/009).

[89] S. Lee, R. Lange, S. Hong, S. Zollner, P. Canfield, A. Panchula, B. Harmon and D. Lynch, *Theoretical and experimental determination of optical and magneto-optical properties of LuFe₂ single crystal*, Thin Solid Films **313-314**, 222 (1998), doi:[https://doi.org/10.1016/S0040-6090\(97\)00822-5](https://doi.org/10.1016/S0040-6090(97)00822-5).

[90] M. V. Berry, *The singularities of light: intensity, phase, polarisation*, Light: Science & Applications **12**(1), 238 (2023), doi:[10.1038/s41377-023-01270-8](https://doi.org/10.1038/s41377-023-01270-8).

[91] J. F. Nye and M. V. Berry, *Dislocations in wave trains*, Proceedings of the Royal Society of London. A. Mathematical and Physical Sciences **336**(1605), 165 (1974), doi:[10.1098/rspa.1974.0012](https://doi.org/10.1098/rspa.1974.0012).

[92] C. J. Glassbrenner and G. A. Slack, *Thermal conductivity of silicon and germanium from 3 K to the melting point*, Phys. Rev. **134**, A1058 (1964).

[93] P. H. Keesom and G. Seidel, *Specific heat of germanium and silicon at low temperatures*, Phys. Rev. **113**, 33 (1959), doi:[10.1103/PhysRev.113.33](https://doi.org/10.1103/PhysRev.113.33).

[94] S. A. Khrapak, *Lindemann melting criterion in two dimensions*, Phys. Rev. Res. **2**, 012040 (2020), doi:[10.1103/PhysRevResearch.2.012040](https://doi.org/10.1103/PhysRevResearch.2.012040).

[95] E. Sjöqvist, *Locality and topology in the molecular Aharonov-Bohm effect*, Phys. Rev. Lett. **89**, 210401 (2002), doi:[10.1103/PhysRevLett.89.210401](https://doi.org/10.1103/PhysRevLett.89.210401).

[96] S. K. Min, A. Abedi, K. S. Kim and E. K. U. Gross, *Is the molecular Berry phase an artifact of the born-oppenheimer approximation?*, Phys. Rev. Lett. **113**, 263004 (2014), doi:[10.1103/PhysRevLett.113.263004](https://doi.org/10.1103/PhysRevLett.113.263004).

[97] M. Berry, *Geometric phase memories*, Nature Physics **6**(3), 148 (2010), doi:[10.1038/nphys1608](https://doi.org/10.1038/nphys1608).